Structure, Magnetism and Thermal Stability of the $n = 3$ Ruddlesden-Popper Oxyfluoride $La_4Ni_3O_{8.4}F_{3.5}$

Supporting information

Jakob Geßner[1], Stefan G. Ebbinghaus[1] and Jonas Jacobs[1,]*

[1] Martin Luther University Halle-Wittenberg, Faculty of Natural Sciences II, Institute of Chemistry, Inorganic Chemistry, Kurt-Mothes-Straße 2, 06120, Halle, Germany

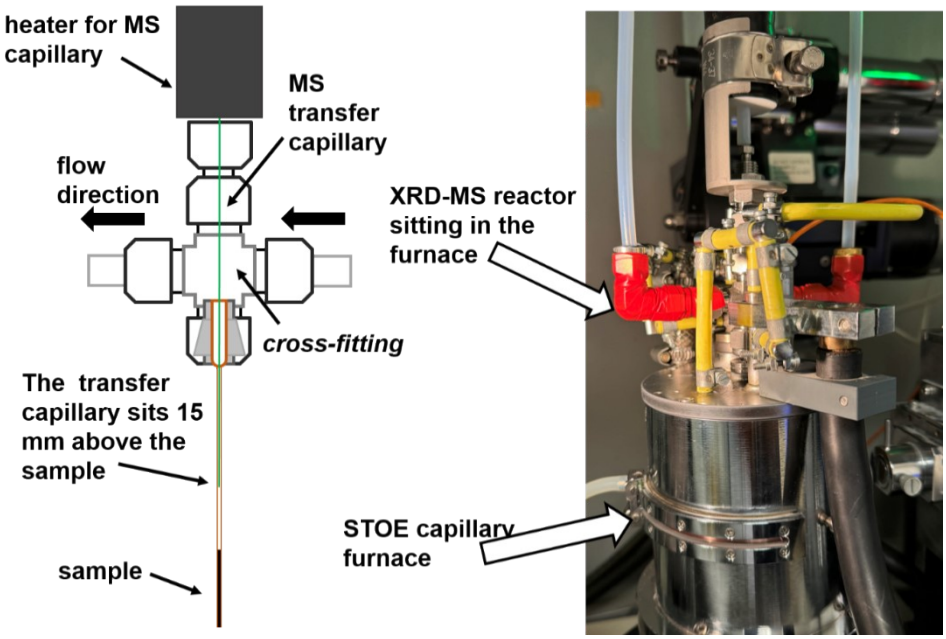

Figure S 1: Sketch of the XRD-MS capillary setup used for investigating the thermal stability of the oxyfluoride, allowing the analysis of gaseous reaction products. On the right, a photograph of the setup in the STOE capillary furnace is shown.

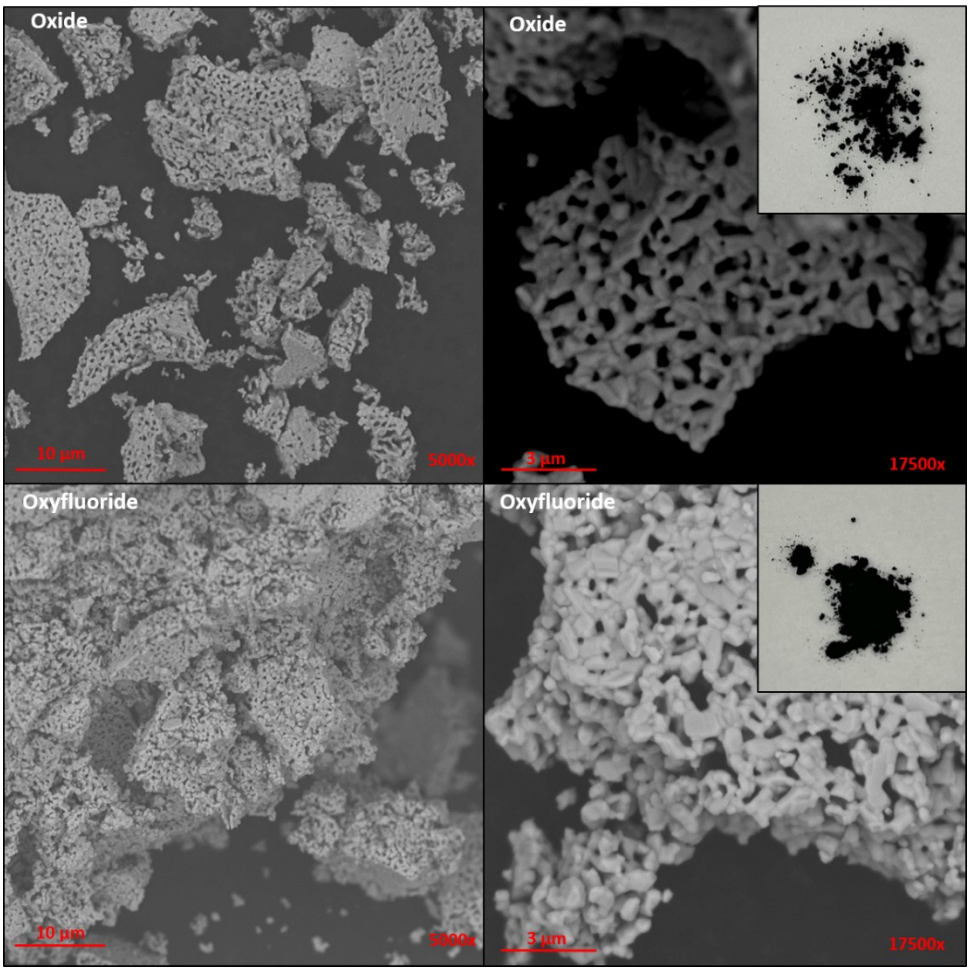

Figure S 2: SEM images of different magnification levels and photographs of both the oxide and the oxyfluoride.

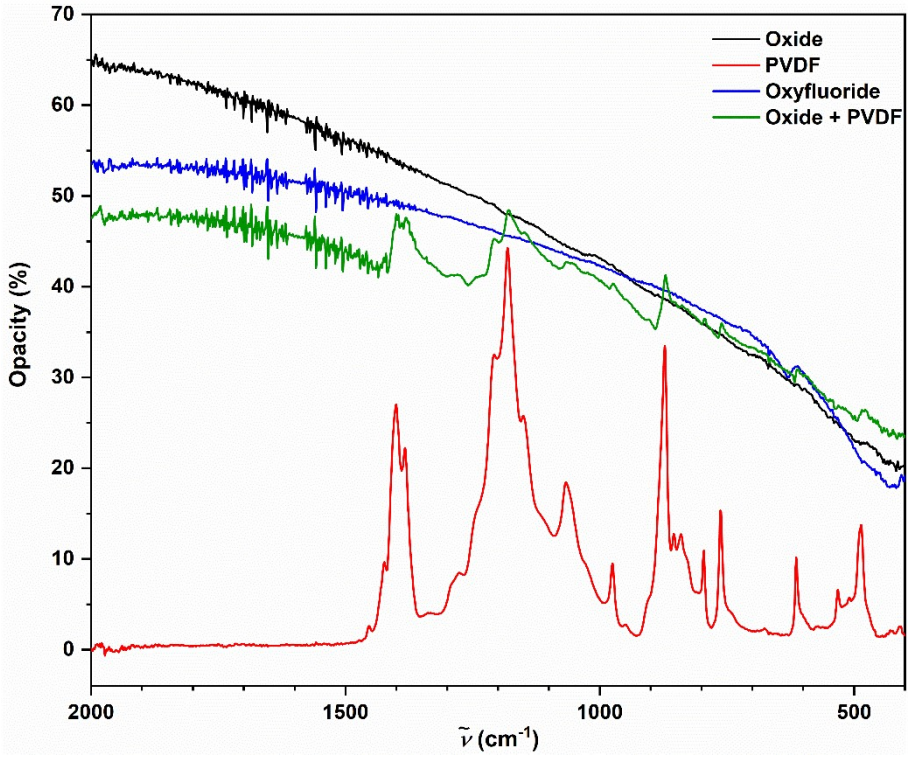

Figure S 3: Infrared spectra of $La_4Ni_3O_{10}$ (black), PVDF (red), $La_4Ni_3O_{8.4}F_{3.5}$ (blue), $La_4Ni_3O_{10}$ + PVDF (green).

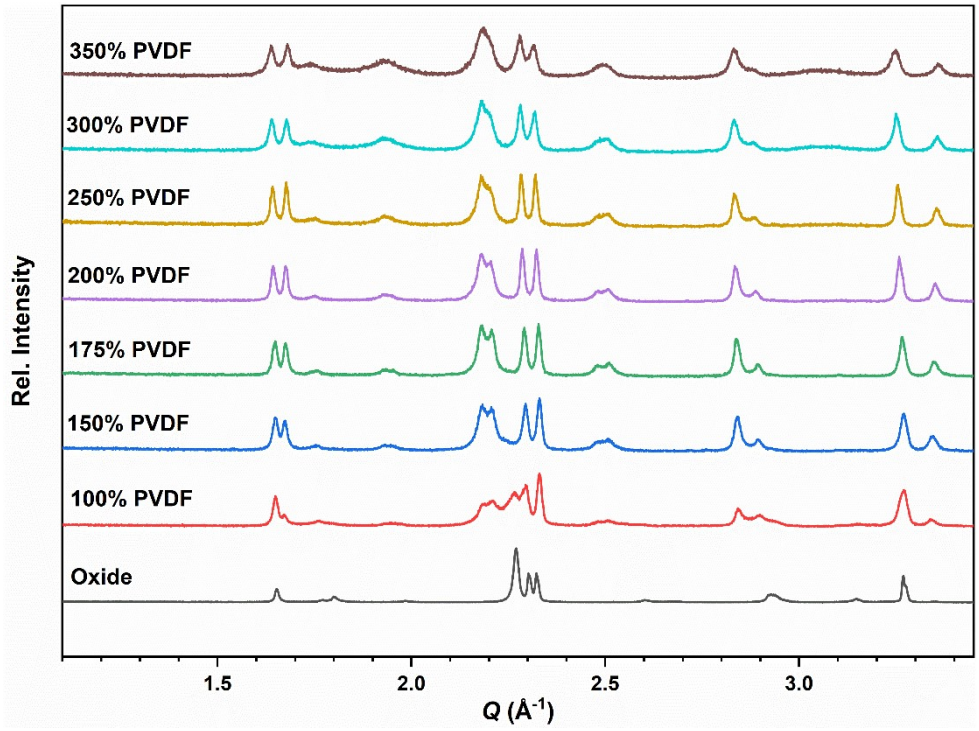

Figure S 4: Diffraction patterns of reaction products from batches with different amounts (mol %) of PVDF used as fluorinating agent. Values refer to the monomeric unit of PVDF with 100% corresponding to the exchange of 1 O^{2-} by 2 F^-.

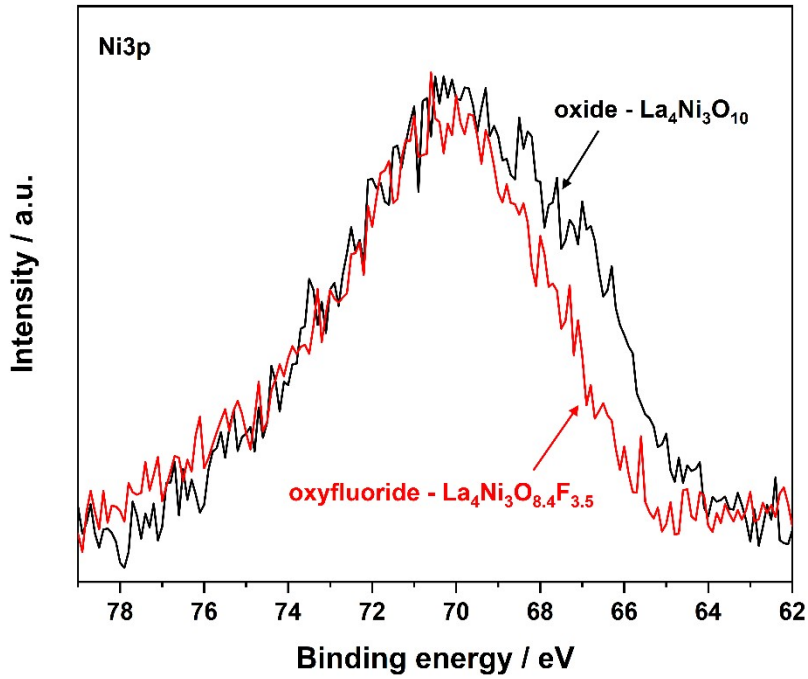

Figure S 5: Ni 3p XPS spectra of $La_4Ni_3O_{10}$ and $La_4Ni_3O_{8.4}F_{3.5}$.

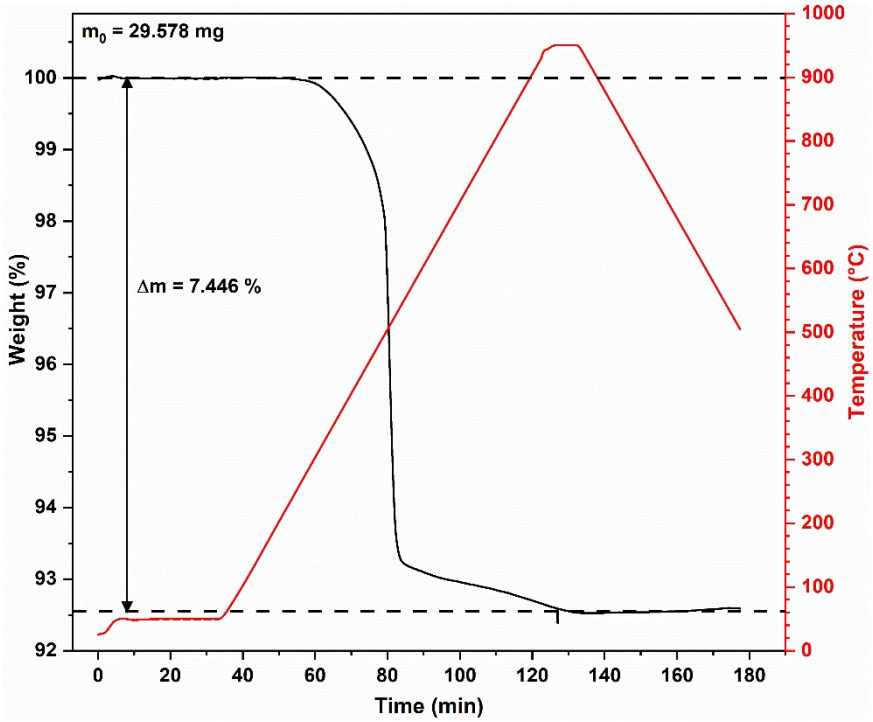

Figure S 6: TGA of the decomposition of $La_4Ni_3O_{8.4}F_{3.5}$ in reducing atmosphere N_2/H_2 (95/5).

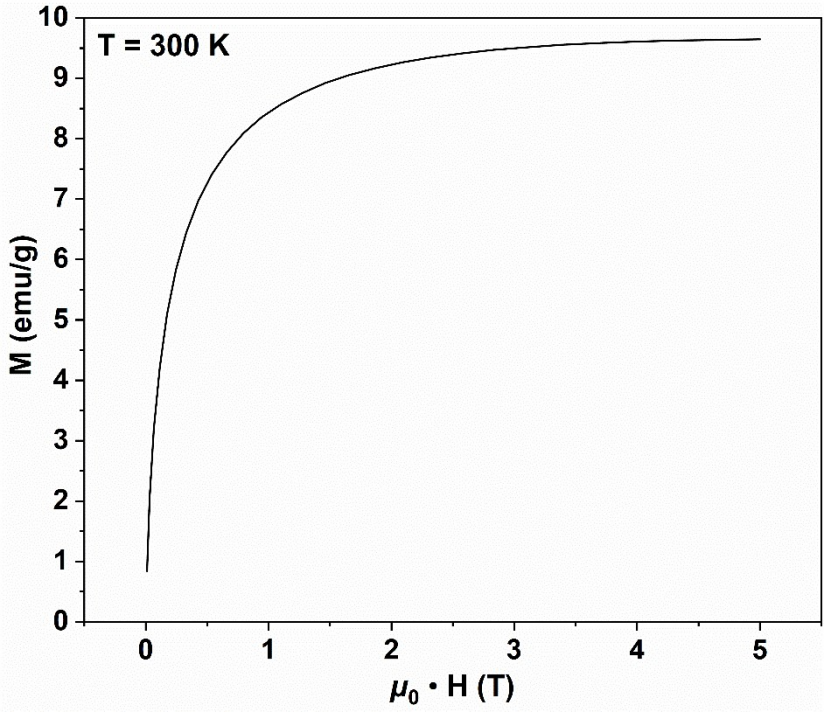

Figure S 7: Field-dependent magnetization data of a sample obtained after the reduction in the TGA. The clear ferromagnetic behavior indicates that the product contains nickel (0).

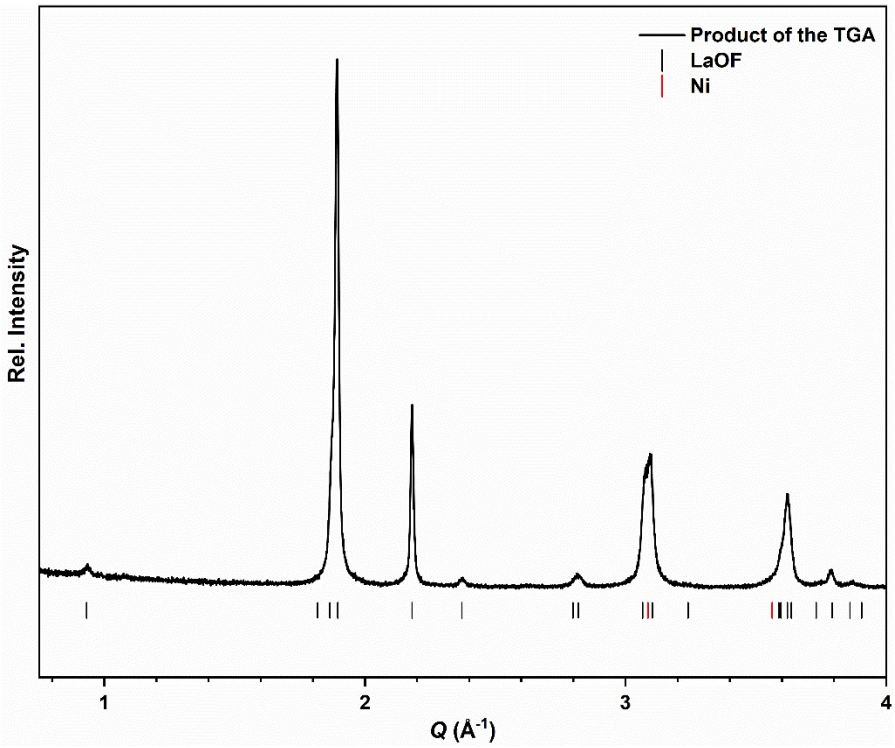

Figure S 8: XRD pattern of the product obtained after the reduction in the TGA (Cu $K_{\alpha 1}$; λ = 1.5406Å).

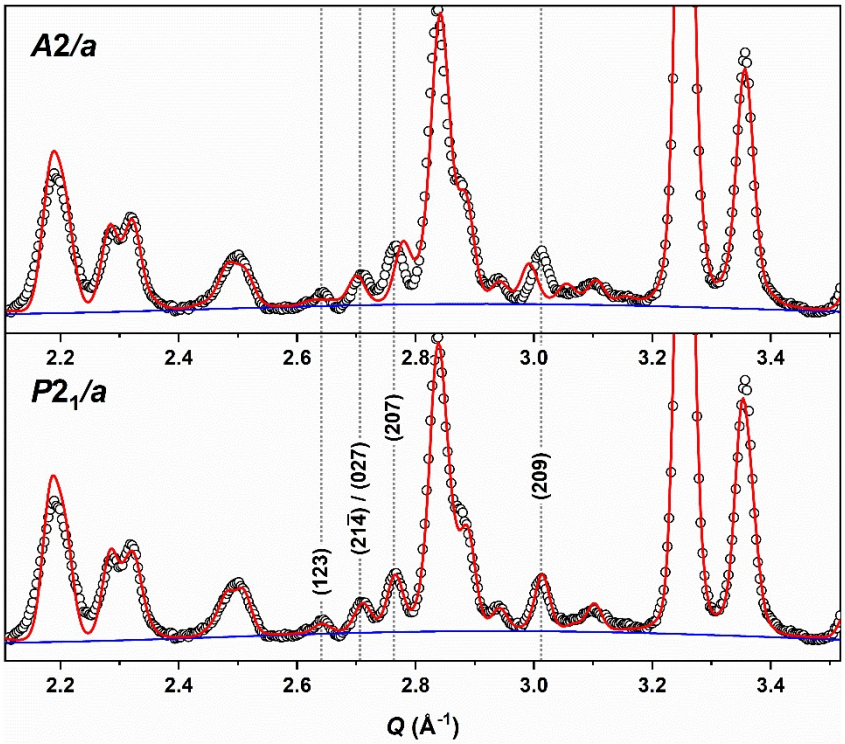

Figure S 9: Le Bail refinements of the NPD data in space groups $A2/a$ and $P2_1/a$. Peaks which cannot be indexed in $A2/a$ are highlighted.

Table S 1: BVS values obtained for different anion distributions. (a) Full statistical distribution of all non-interstitial F^- (15% per site). (b) Occupation of the O/F(6) site solely by F^- and statistical distribution of the remaining F^- to all other anion sites (5.55% per site), (c) Full occupation of O/F(6) by F^-, and O/F(5) by O^{2-} and statistical distribution of the remaining F^- to all other anion sites (6.25% per site). (d) O/F(5), and O/F(6) occupied like in (c) but partly occupation of O/F(1) and O/F(4) by F^- (25% per site). (e) O/F(5), and O/F(6) occupied like in (c) and partly occupation of O/F(9) and O/F(10) by F^- (25% per site).

Atom	(a)	(b)	(c)	(d)	(e)
	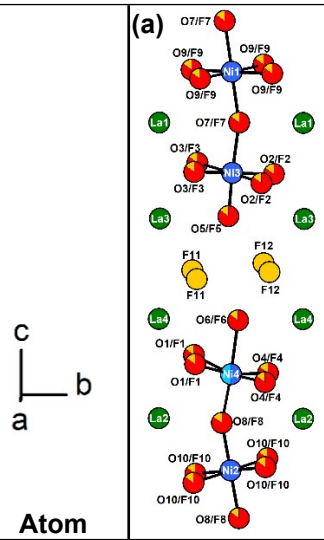	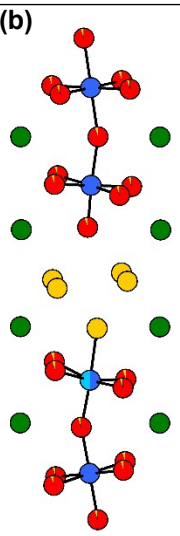	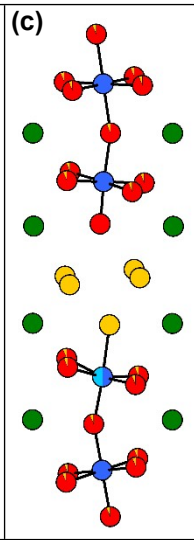	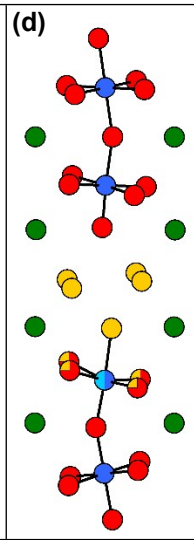	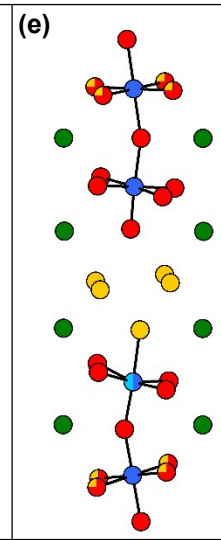
La^{3+} (1)	2.8	2.9	2.9	2.9	2.9
La^{3+} (2)	2.8	2.9	2.9	2.9	2.9
La^{3+} (3)	3.2	3.3	3.3	3.3	3.3
La^{3+} (4)	2.9	2.7	2.7	2.7	2.7
Ni^{3+} (1)	2.7	2.8	2.8	2.8	2.7
Ni^{3+} (2)	3.1	3.1	3.1	3.2	3.1
Ni^{3+} (3)	3.4	3.4	3.4	3.5	3.5
Ni^{2+} (4a)	2.6	2.6	2.6	2.5	2.5
Ni^{3+} (4b)	2.5	2.5	2.5	2.4	2.7
O^{2-} (1)	1.9	1.9	1.9	1.9	1.9
F^{1-} (1)	1.5	1.5	1.5	1.5	--
O^{2-} (2)	2.3	2.3	2.3	2.3	2.3
F^{1-} (2)	1.6	1.6	1.6	--	--
O^{2-} (3)	2.0	2.0	2.0	2.0	2.0
F^{1-} (3)	1.5	1.5	1.5	--	--
O^{2-} (4)	2.1	2.1	2.1	2.1	2.1
F^{1-} (4)	1.6	1.6	1.6	1.6	--
O^{2-} (5)	1.9	1.9	1.9	1.9	1.9
F^{1-} (5)	1.5	1.5	--	--	--
O^{2-} (6)	1.3	--	--	--	--
F^{1-} (6)	1.0	1.0	1.0	1.0	1.0
O^{2-} (7)	2.0	2.0	2.0	2.0	2.0
F^{1-} (7)	1.4	1.4	1.4	--	--
O^{2-} (8)	2.2	2.2	2.2	2.2	2.2
F^{1-} (8)	1.6	1.6	1.6	--	--
O^{2-} (9)	1.9	1.9	1.9	1.9	1.9
F^{1-} (9)	1.4	1.4	1.4	--	1.4
O^{2-} (10)	1.8	1.8	1.8	1.8	1.8
F^{1-} (10)	1.4	1.4	1.4	--	1.4
F^{1-} (11)	0.9	0.9	0.9	0.9	0.9
F^{1-} (12)	0.9	0.9	0.9	0.9	0.9
GII	**11.0%**	**7.8%**	**7.9%**	**8.2%**	**7.7%**

Table S 2: Bond distances extracted from Rietveld refinement of $La_4Ni_3O_{8.4}F_{3.5}$ (compare Figure S 7).

Bond	Distance [Å]	Bond	Distance [Å]	Bond	Distance [Å]
La(1) – O/F(2)	2.655(1)	La(3) – O/F(2)	2.324(1)	Ni(1) – O/F(7)	1.981(1)
La(1) – O/F(2)	3.070(1)	La(3) – O/F(2)	2.668(1)	Ni(1) – O/F(7)	1.982(1)
La(1) – O/F(3)	2.593(1)	La(3) – O/F(3)	2.689(1)	Ni(1) – O/F(9)	1.940(1)
La(1) – O/F(3)	2.594(1)	La(3) – O/F(3)	2.813(1)	Ni(1) – O/F(9)	1.940(1)
La(1) – O/F(7)	2.452(1)	La(3) – O/F(5)	2.617(1)	Ni(1) – O/F(9)	1.966(1)
La(1) – O/F(7)	2.695(2)	La(3) – O/F(5)	2.658(2)	Ni(1) – O/F(9)	1.966(1)
La(1) – O/F(7)	2.751(2)	La(3) – O/F(5)	2.771(2)	Ni(2) – O/F(8)	1.863(1)
La(1) – O/F(7)	3.056(2)	La(3) – O/F(5)	2.895(1)	Ni(2) – O/F(8)	1.863(1)
La(1) – O/F(9)	2.524(1)	La(3) – F(1)	2.591(1)	Ni(2) – O/F(10)	1.954(1)
La(1) – O/F(9)	2.623(1)	La(3) – F(1)	2.703(1)	Ni(2) – O/F(10)	1.954(1)
La(1) – O/F(9)	2.920(1)	La(3) – F(2)	2.464(1)	Ni(2) – O/F(10)	1.958(1)
La(1) – O/F(9)	3.000(1)	La(3) – F(2)	2.544(1)	Ni(2) – O/F(10)	1.958(1)
La(2) – O/F(1)	2.964(1)	La(4) – O/F(1)	2.420(1)	Ni(3) – O/F(2)	1.897(1)
La(2) – O/F(1)	2.966(1)	La(4) – O/F(1)	2.526(1)	Ni(3) – O/F(2)	1.996(1)
La(2) – O/F(4)	2.485(1)	La(4) – O/F(4)	2.907(1)	Ni(3) – O/F(3)	1.954(1)
La(2) – O/F(4)	2.523(1)	La(4) – O/F(4)	3.027(1)	Ni(3) – O/F(3)	1.957(1)
La(2) – O/F(8)	2.413(1)	La(4) – O/F(6)	2.484(1)	Ni(3) – O/F(5)	1.682(1)
La(2) – O/F(8)	2.704(2)	La(4) – O/F(6)	2.586(1)	Ni(3) – O/F(7)	1.941(1)
La(2) – O/F(8)	2.764(2)	La(4) – O/F(6)	2.871(2)	Ni(4) – O/F(1)	1.980(1)
La(2) – O/F(8)	3.107(2)	La(4) – O/F(6)	3.032(2)	Ni(4) – O/F(1)	2.065(1)
La(2) – O/F(10)	2.580(1)	La(4) – F(1)	2.520(1)	Ni(4) – O/F(4)	1.918(1)
La(2) – O/F(10)	2.585(1)	La(4) – F(1)	2.622(1)	Ni(4) – O/F(4)	1.930(1)
La(2) – O/F(10)	2.987(1)	La(4) – F(2)	2.585(1)	Ni(4) – O/F(6)	2.098(1)
La(2) – O/F(10)	3.021(1)	La(4) – F(2)	2.948(1)	Ni(4) – O/F(8)	1.907(1)

Table S 3: Bond angles in the $Ni(O,F)_6$ octahedra of $La_4Ni_3O_{8.4}F_{3.5}$ extracted from Rietveld refinement. For assignment of the different sites compare Figure S 7.

Atom A	Atom B	Atom C	Angle B-A-C [°]	Atom A	Atom B	Atom C	Angle B-A-C [°]
Ni(1)	O/F(9)	O/F(9)	180.0(1)	Ni(3)	O/F(5)	O/F2	87.4(3)
Ni(1)	O/F(9)	O/F(9)	91.1(1)	Ni(3)	O/F(5)	O/F(7)	175.2(6)
Ni(1)	O/F(9)	O/F(9)	88.9(1)	Ni(3)	O/F(5)	O/F(3)	92.6(3)
Ni(1)	O/F(9)	O/F(7)	86.2(2)	Ni(3)	O/F(5)	O/F(3)	92.0(3)
Ni(1)	O/F(9)	O/F(7)	93.8(2)	Ni(3)	O/F(5)	O/F(2)	87.8(3)
Ni(1)	O/F(9)	O/F(9)	88.9(1)	Ni(3)	O/F(2)	O/F(7)	93.9(2)
Ni(1)	O/F(9)	O/F(9)	91.1(1)	Ni(3)	O/F(2)	O/F(3)	85.8(1)
Ni(1)	O/F(9)	O/F(7)	93.8(2)	Ni(3)	O/F(2)	O/F(3)	173.5(1)
Ni(1)	O/F(9)	O/F(7)	86.2(2)	Ni(3)	O/F(2)	O/F(2)	89.6(1)
Ni(1)	O/F(9)	O/F(9)	180	Ni(3)	O/F(7)	O/F(3)	92.2(2)
Ni(1)	O/F(9)	O/F(7)	93.4(2)	Ni(3)	O/F(7)	O/F(3)	87.2(2)
Ni(1)	O/F(9)	O/F(7)	86.6(2)	Ni(3)	O/F(7)	O/F(2)	87.5(2)
Ni(1)	O/F(9)	O/F(7)	86.6(2)	Ni(3)	O/F(3)	O/F(3)	87.8(1)
Ni(1)	O/F(9)	O/F(7)	93.4(2)	Ni(3)	O/F(3)	O/F(2)	175.3(1)
Ni(1)	O/F(7)	O/F(7)	180	Ni(3)	O/F(3)	O/F(2)	96.9(1)
Ni(2)	O/F(8)	O/F(8)	180	Ni(4)	O/F(8)	O/F(4)	93.7(2)
Ni(2)	O/F(8)	O/F(10)	91.4(2)	Ni(4)	O/F(8)	O/F(4)	93.8(2)
Ni(2)	O/F(8)	O/F(10)	88.6(2)	Ni(4)	O/F(8)	O/F(1)	98.8(2)
Ni(2)	O/F(8)	O/F(10)	88.1(2)	Ni(4)	O/F(8)	O/F(1)	97.8(2)
Ni(2)	O/F(8)	O/F(10)	91.9(2)	Ni(4)	O/F(8)	O/F(6)	176.4(5)
Ni(2)	O/F(8)	O/F(10)	88.6(2)	Ni(4)	O/F(4)	O/F(4)	89.6(1)
Ni(2)	O/F(8)	O/F(10)	91.4(2)	Ni(4)	O/F(4)	O/F(1)	90.2(1)
Ni(2)	O/F(8)	O/F(10)	91.9(2)	Ni(4)	O/F(4)	O/F(1)	167.9(1)
Ni(2)	O/F(8)	O/F(10)	88.2(2)	Ni(4)	O/F(4)	O/F(6)	87.1(2)
Ni(2)	O/F(10)	O/F(10)	180.0(1)	Ni(4)	O/F(4)	O/F(1)	167.4(1)
Ni(2)	O/F(10)	O/F(10)	92.3(1)	Ni(4)	O/F(4)	O/F(1)	93.6(1)
Ni(2)	O/F(10)	O/F(10)	87.7(1)	Ni(4)	O/F(4)	O/F(6)	89.7(2)
Ni(2)	O/F(10)	O/F(10)	87.7(1)	Ni(4)	O/F(1)	O/F(1)	84.2(1)
Ni(2)	O/F(10)	O/F(10)	92.3(1)	Ni(4)	O/F(1)	O/F(6)	77.7(2)
Ni(2)	O/F(10)	O/F(10)	180	Ni(4)	O/F(1)	O/F(6)	81.3(2)
O/F(7)	Ni(1)	Ni(3)	163.5(5)	O/F(8)	Ni(4)	Ni(2)	159.2(7)

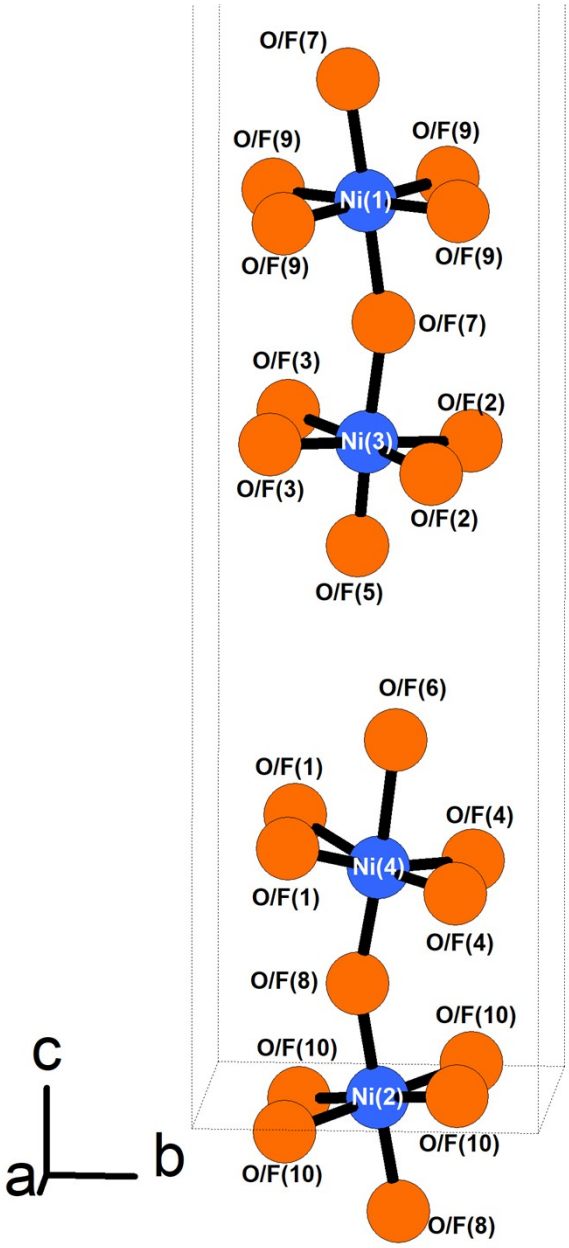

Figure S 10: Detailed representation of the four different $Ni(O,F)_6$ octahedra in $La_4Ni_3O_{8.4}F_{3.5}$. Note that the picture only shows a small part of the unit cell (compare Figure 5). Distortions of the terminal octahedra (around Ni(3) and Ni(4)) are clearly visible.

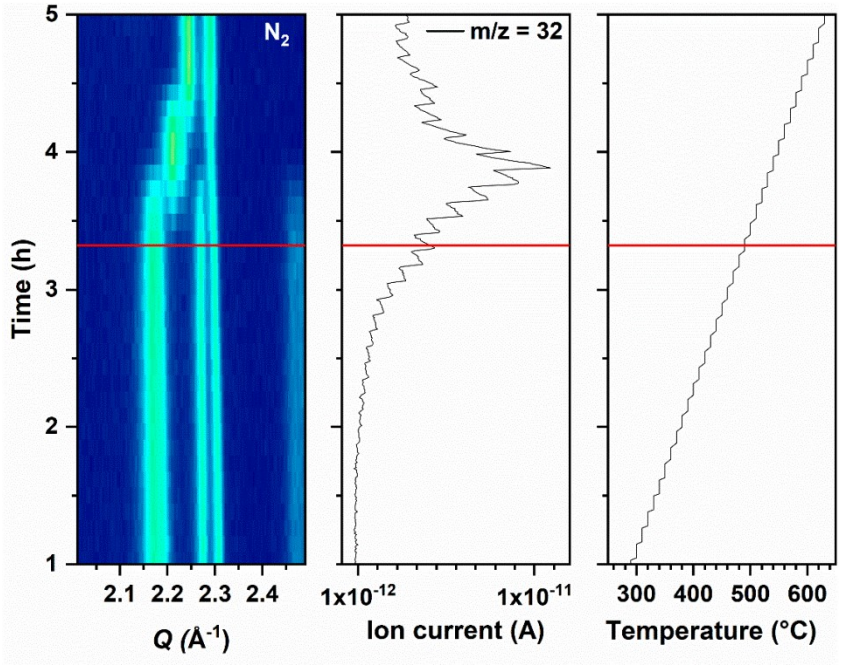

Figure S 11: XRD-MS data during the decomposition of $La_4Ni_3O_{8.4}F_{3.5}$ in flowing N_2. The red lines are a guide to the eye for the temperature of 490 °C. A clear increase of the O_2 signal in the region of the formation of the decomposition intermediate is found.

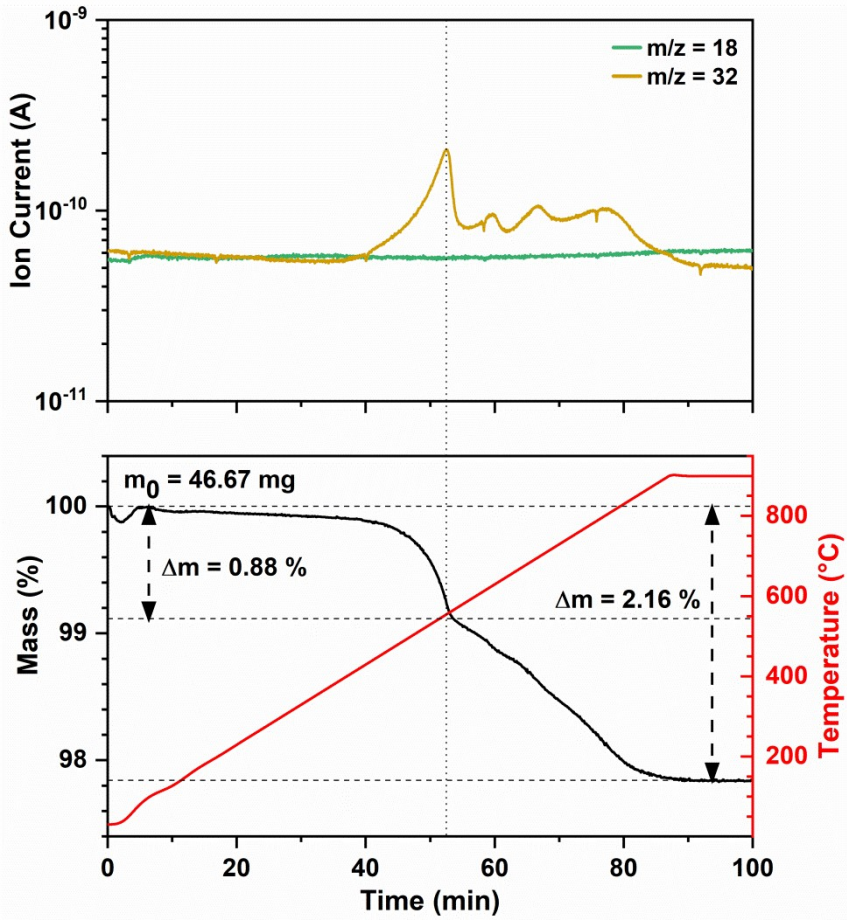

Figure S 12: TG-MS data for the decomposition of $La_4Ni_3O_{8.4}F_{3.5}$ in flowing N_2. The dotted lines serve as guide to the eye.

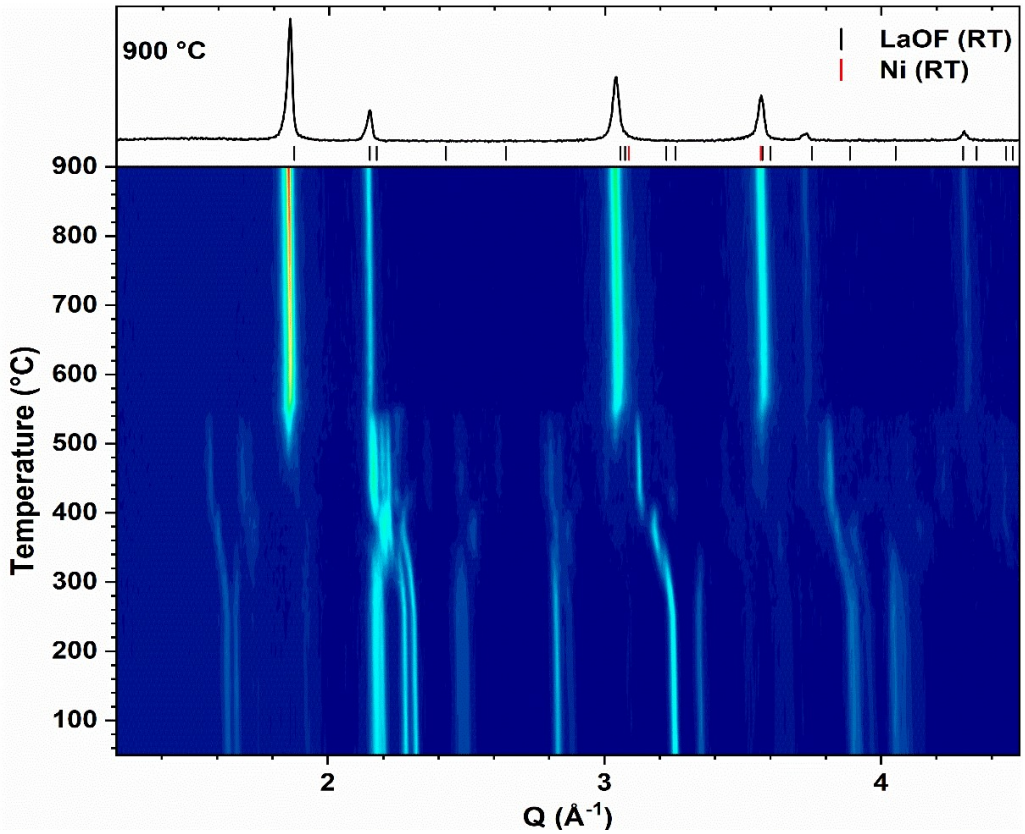

Figure S 13: Contour plot of the *in situ* XRD patterns obtained for the thermal decomposition of $La_4Ni_3O_{8.4}F_{3.5}$ in reducing atmosphere (10% H_2 in N_2). The final pattern is plotted in the upper part of the figure and the positions of Bragg reflections for LaOF and Ni are shown (please note that the reference data is obtained at room temperature).

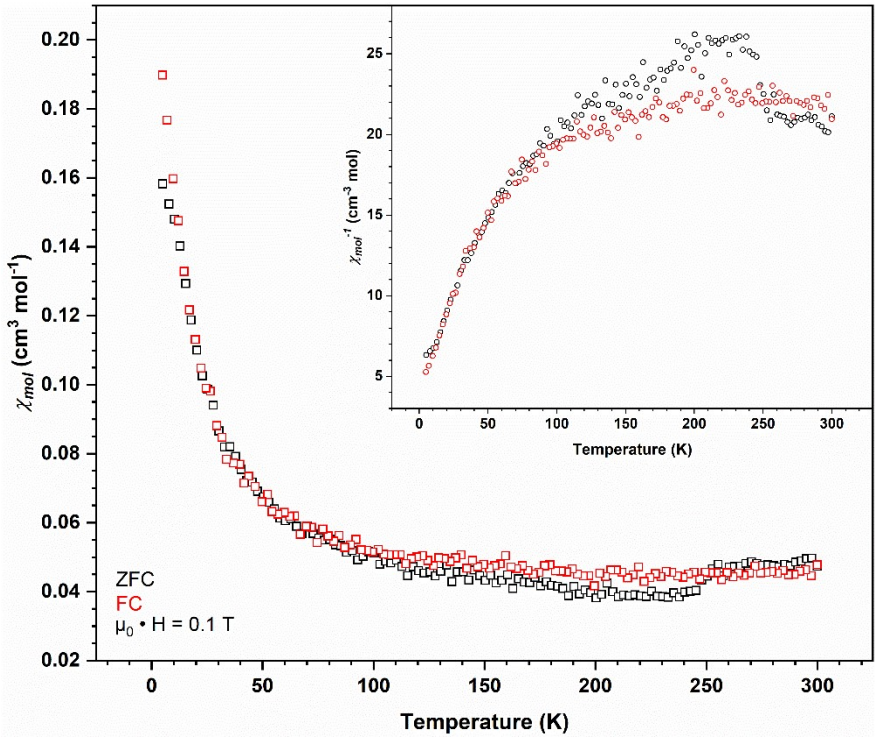

Figure S 14: Temperature dependent susceptibility and inverse susceptibility (inset) of $La_4Ni_3O_{8.4}F_{3.5}$ at 0.1 T for field cooled (red) and zero-field cooled (black) conditions. Due to the large noise level no Curie-Weiss fits were applied.